

## **Electronic transitions of tetrathiafulvalene oriented in polyethylene film**

Near and vacuum UV synchrotron radiation polarization spectroscopy

Thulstrup, Peter Waaben; Hoffmann, Søren Vrønning; Jones, Nikola Clare; Spanget-Larsen, Jens

*Published in:*  
Chemical Physics Impact

*DOI:*  
[10.1016/j.chphi.2020.100009](https://doi.org/10.1016/j.chphi.2020.100009)

*Publication date:*  
2021

*Document Version*  
Publisher's PDF, also known as Version of record

### *Citation for published version (APA):*

Thulstrup, P. W., Hoffmann, S. V., Jones, N. C., & Spanget-Larsen, J. (2021). Electronic transitions of tetrathiafulvalene oriented in polyethylene film: Near and vacuum UV synchrotron radiation polarization spectroscopy. *Chemical Physics Impact*, 2(June 2021), Article 100009.  
<https://doi.org/10.1016/j.chphi.2020.100009>

### **General rights**

Copyright and moral rights for the publications made accessible in the public portal are retained by the authors and/or other copyright owners and it is a condition of accessing publications that users recognise and abide by the legal requirements associated with these rights.

- Users may download and print one copy of any publication from the public portal for the purpose of private study or research.
- You may not further distribute the material or use it for any profit-making activity or commercial gain.
- You may freely distribute the URL identifying the publication in the public portal.

### **Take down policy**

If you believe that this document breaches copyright please contact [rucforsk@kb.dk](mailto:rucforsk@kb.dk) providing details, and we will remove access to the work immediately and investigate your claim.



# Electronic transitions of tetrathiafulvalene oriented in polyethylene film. Near and vacuum UV synchrotron radiation polarization spectroscopy

P.W. Thulstrup<sup>a,\*</sup>, S.V. Hoffmann<sup>b</sup>, N.C. Jones<sup>b</sup>, J. Spanget-Larsen<sup>c,\*</sup>

<sup>a</sup> Department of Chemistry, University of Copenhagen, Universitetsparken 5, DK-2100 Copenhagen, Denmark

<sup>b</sup> ISA, Department of Physics and Astronomy, Aarhus University, Ny Munkegade 120, Building 1520, DK-8000 Aarhus C, Denmark

<sup>c</sup> Department of Science and Environment, Roskilde University, P.O.Box 260, DK-4000 Roskilde, Denmark

## ARTICLE INFO

### Keywords:

Tetrathiafulvalene  
Linear dichroism  
Polarization direction  
Electronic transition  
Synchrotron radiation  
UV spectroscopy

## ABSTRACT

The electronic spectrum of tetrathiafulvalene (TTF) oriented in a polyethylene film is characterized experimentally using synchrotron radiation linear dichroism from the near-UV to the vacuum-UV region to 56,500 cm<sup>-1</sup> (177 nm). The non-planar TTF molecule is shown to have electronic transitions of significant intensity polarized along all three molecular symmetry axes. A procedure for processing linear dichroic data to obtain partial absorbance curves representing different polarization directions is exemplified. The overlapping contributions to eight individual spectral features are furthermore interpreted by the aid of time-dependent density functional theory using CAM-B3LYP/6-311++G(3df,3pd) with geometry optimized at the B3LYP / 6-311++G(3df,3pd) level within the C<sub>2v</sub> point group. Additional calculations using larger basis sets as well as other long-range corrected functionals (LC- $\omega$ PBE and  $\omega$ B97XD) yielded similar results. The planar conformer with D<sub>2h</sub> symmetry is also considered and it is discussed that rapid equilibration via this transition state may contribute to the diffuse nature of some features of the electronic spectrum. The TTF molecule is a dynamic and 3-dimensional chromophore, and these characteristics may serve as a basis for understanding the optical properties of the numerous TTF-based materials finding applications in supramolecular chemistry, molecular electronics and beyond.

## 1. Introduction

The tetrathiafulvalene (TTF, Scheme 1) motif is renowned for its role in Bechgaard salts [1,2]. These are organic superconductors that rely on charge-transfer complexes comprised of a TTF derived radical cation and an anion, which in the solid state can display low-temperature superconductivity. TTF itself is non-aromatic and non-planar, its stable geometry being a boat-like conformation of C<sub>2v</sub> symmetry. The compound has remarkable redox properties, and the aromatic radical cation and di-cation forms are readily obtained reversibly, the former being planar with D<sub>2h</sub> symmetry, and the latter twisted along the central bond with D<sub>2</sub> symmetry. Prior to Bechgaard salts being characterized, numerous examples of conducting TTF materials were described and explored for their electrically conducting properties, see an overview by Martin [3]. TTF is also intrinsically connected with the term *molecular electronics* and with so-called Aviram–Ratner Rectifiers that were proposed in a seminal paper in 1974 [4]. Such compounds where a TTF donor is connected with an acceptor by a  $\sigma$ -bonded bridge have since been experimentally characterized; see for instance Ho et al. [5]. TTF has also had a prominent role in supramolecular chemistry and for construction of mechanically in-

terlocked molecules, electrochromic materials, molecular switches and machines, where functionality can be incorporated by virtue of the electron donor capability of TTF derivatives and their ability to engage in donor-acceptor complexes with electron acceptors [6–9].

The electronic structure of TTF has been investigated by several workers [10–17]. In this publication, we report the results of an experimental and theoretical study of the excited electronic states of TTF. The electronic absorption spectrum is investigated by Synchrotron Radiation Linear Dichroism (SRLD) spectroscopy in the range 56,500 – 20,000 cm<sup>-1</sup> (177 – 400 nm) on molecular samples partially aligned in stretched polyethylene (PE). LD spectroscopy on an ordered molecular assembly enables elucidation of otherwise unresolved spectral features and provides information on the moment directions of the observed transitions [18–23]. TTF turns out to be a truly three-dimensional chromophore, with overlapping contributions from intensity polarized along all three symmetry axes of the chromophore, a situation which complicates the interpretation of the LD spectra in terms of partial absorbance curves. We shall show that the construction of so-called reduced absorbance curves provides a useful representation of the experimental polarization spectra, revealing previously unrecognized features. The observed

Abbreviations: TTF, Tetrathiafulvalene; SRLD, Synchrotron Radiation Linear Dichroism; PE, Polyethylene.

\* Corresponding authors.

E-mail addresses: [pwt@chem.ku.dk](mailto:pwt@chem.ku.dk) (P.W. Thulstrup), [spanget@ruc.dk](mailto:spanget@ruc.dk) (J. Spanget-Larsen).

<https://doi.org/10.1016/j.chphi.2020.100009>

Received 27 October 2020; Received in revised form 11 December 2020; Accepted 11 December 2020

2667-0224/© 2020 The Author(s). Published by Elsevier B.V. This is an open access article under the CC BY license (<http://creativecommons.org/licenses/by/4.0/>)

absorbance bands are compared with theoretical transitions predicted with Time Dependent Density Functional Theory (TD-DFT) [24–26] using different functionals and basis sets. Additional information is provided as Supplementary data, referred to in the ensuing text as S1 – S11.

## 2. Experimental

### 2.1. Materials

Tetrathiafulvalene (TTF) [31366-25-3] (97%) was obtained as a red solid from Sigma-Aldrich (Aldrich cat. no. 183180). Polyethylene films (PE) were pure low-density PE sheet material (Hinnum Plast, DK-2670 Greve, Denmark). Chloroform was spectroscopic grade (Uvasol)  $\text{CHCl}_3$  from Sigma-Aldrich.

### 2.2. Sample preparation

For UV measurements a PE sheet of approximately 100  $\mu\text{m}$  thickness (prior to stretching) was soaked briefly in a chloroform solution containing TTF, while a reference sheet was soaked in pure chloroform. The chloroform was subsequently allowed to evaporate from the PE sheets in a fume hood. The film surfaces were cleaned with methanol to remove any crystalline deposits of TTF. The resulting sample thus consisted of TTF solubilized inside the PE sheets. For linear dichroism (LD) measurements, the polymer was stretched uniaxially approximately by 500% in an in-house constructed apparatus. All sample manipulations were performed at room temperature and ambient pressure. Additional information on stretched polyethylene samples can be found in the literature [18–23].

### 2.3. Synchrotron radiation UV linear dichroism

Synchrotron radiation LD spectra were measured at room temperature as previously described [27–34] on the UV beamline [35–37] at the storage ring ASTRID2 at the Centre for Storage Ring Facilities (ISA), Aarhus University, Denmark. The synchrotron beamline provides a much higher photon flux in the far UV spectral range compared to a conventional light source. This yields an improved signal to noise ratio, as well as extending the accessible wavenumber range for PE samples up to at least  $56,000\text{ cm}^{-1}$ . Data were recorded in the  $500\text{ nm} - 177\text{ nm}$  ( $\sim 56,500\text{ cm}^{-1}$ ) range with one point per nm. The baseline-corrected LD absorbance curves are denoted  $E_U(\tilde{\nu})$  and  $E_V(\tilde{\nu})$  and correspond to parallel and perpendicular polarization of the radiation with respect to the uniaxial stretching direction  $U$  of the polymer sample. To minimize problems due to evaporation of TTF from the PE sample during the measurements, the sample curves were recorded in the following sequence: first  $E_V(\tilde{\nu})$ , then  $E_U(\tilde{\nu})$ , and then again  $E_V(\tilde{\nu})$ , immediately after one another. For definition of the LD, the average of the two  $E_V(\tilde{\nu})$  absorbance measurements was taken and compared with the intermediate  $E_U(\tilde{\nu})$  spectrum. The resulting LD curves are shown in Fig. 1, top.

## 3. Density functional theoretical calculations

Quantum chemical calculations were performed with the GAUSSIAN09 [38] and GAUSSIAN16 [39] software packages. The ground state geometry of TTF was computed by using B3LYP [40,41] DFT and the 6-311++G(3df,3pd) basis set [38,39]. The molecule is predicted to have a  $C_{2v}$  symmetrical boat-shaped nuclear equilibrium configuration, consistent with the results of previous experimental and theoretical investigations [15–17,42–44]. The planar  $D_{2h}$  symmetrical configuration is predicted to be a transition structure, interrelating two equivalent boat-shaped structures; the electronic energy barrier is computed to be 0.08 kcal/mol. The computed nuclear coordinates and molecular energies for the  $C_{2v}$  and  $D_{2h}$  structures are provided as Supplementary data S1 and S2. Vertical electronic transitions from the ground state to the

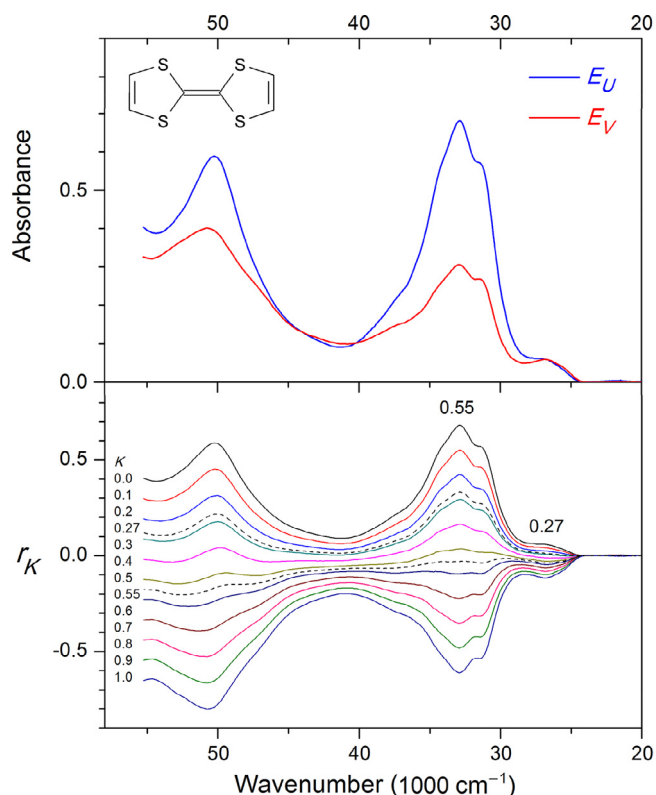


**Fig. 1.** Top: Experimental UV synchrotron radiation polarization spectra of TTF oriented in a polyethylene film.  $E_U(\tilde{\nu})$  and  $E_V(\tilde{\nu})$  denote absorbance measured with the beam polarization parallel and perpendicular to the stretching axis  $U$  of the sample. Bottom: Linear combinations  $r_K(\tilde{\nu}) = (1 - K)E_U(\tilde{\nu}) - 2KE_V(\tilde{\nu})$  of the spectra, allowing assignment of  $K$ -values (see text).

50 lowest excited singlet states were computed with the TD-DFT procedure [24–26] using the long range-corrected functional CAM-B3LYP [45] and the 6-311++G(3df,3pd) basis set [38,39]. The main calculated transitions are listed in Table 1 and shown graphically in Fig. 2 (bottom); full listings are provided as Supplementary data S3 and S4. A constant value of  $3000\text{ cm}^{-1}$  was subtracted from the computed wavenumbers to facilitate comparison of observed and predicted trends [32–34]. A comparison of transitions predicted for boat-shape and planar TTF is provided in S5, and results obtained with and without diffuse functions in the basis set are compared in S6. Some important orbitals are shown in Fig. 3. The TD-CAM-B3LYP calculations for boat-shape TTF were repeated with the larger basis sets AUG-cc-pVTZ and AUG-cc-pVQZ [46,47] and additional TD-DFT calculations were performed with the long-range corrected functionals LC- $\omega$ PBE [48,49] and  $\omega$ B97XD [50], all yielding rather similar results (S7 – S11). Convolutions of the predicted transitions were performed by assigning a Gaussian function to each excitation wavenumber with an area proportional to the oscillator strength of that transition, using a constant width parameter,  $\sigma = 1500\text{ cm}^{-1}$ .

## 4. Results and discussion

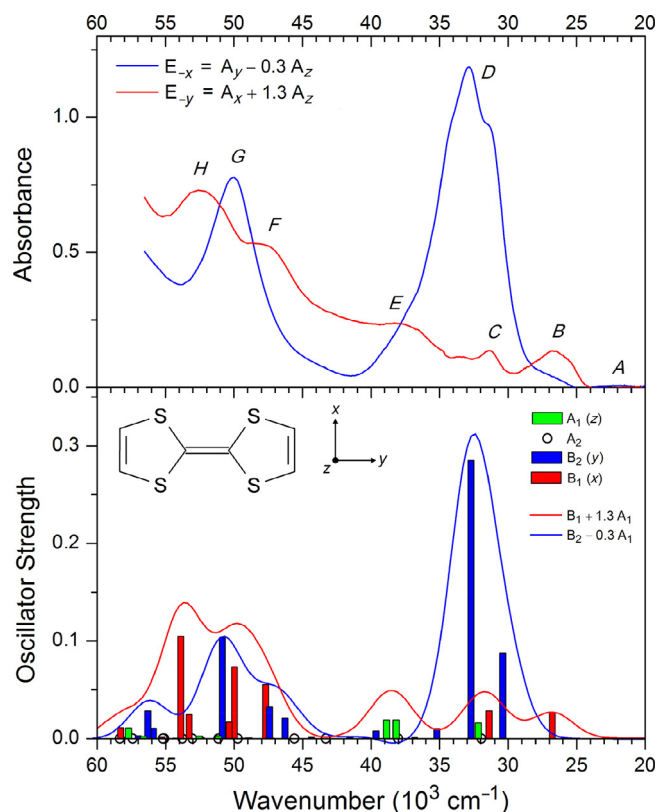
### 4.1. Linear dichroism: orientation factors and partial absorbance curves

The observed LD absorption curves  $E_U(\tilde{\nu})$  and  $E_V(\tilde{\nu})$  for TTF partially aligned in stretched PE are shown in Fig. 1 (top). They are consistent with those measured in the Near-UV region ( $40,000 - 20,000\text{ cm}^{-1}$ ) in a similar experiment by Gleiter et al. [12]. However, our analysis of the observed linear dichroism data differs considerably from that of Gleiter et al. Most significantly, in the present study TTF is recognized and treated explicitly as a three-dimensional chromophore.

**Table 1**

Observed features of the SRLD spectrum of tetrathiafulvalene (TTF) and electronic transitions predicted with TD-CAM-B3LYP.

| Observed |                            |                  |                  | $C_{2v}$ boat-shape configuration <sup>a</sup> |                              |                   |                                     | $D_{2h}$ planar configuration <sup>a</sup> |                              |                   |                                     |
|----------|----------------------------|------------------|------------------|--|------------------------------|-------------------|-------------------------------------|--|------------------------------|-------------------|-------------------------------------|
|          | $\tilde{\nu}$ <sup>b</sup> | Abs <sup>c</sup> | Pol <sup>d</sup> | Term   | $\tilde{\nu}$ <sup>b,e</sup> | $f$ <sup>f</sup>  | Leading configurations <sup>g</sup> | Term                                       | $\tilde{\nu}$ <sup>b,e</sup> | $f$ <sup>f</sup>  | Leading configurations <sup>g</sup> |
| A        | 22.0                       | –                | –                | 2 $^1A_1$ (z)                                  | 21.0                         | $4 \cdot 10^{-4}$ | 78% (1,-1); 18% (1,-4)              | 1 $^1B_{1u}$ (z)                           | 20.1                         | $6 \cdot 10^{-4}$ | 80% (1,-1); 16% (1,-3)              |
| B        | 26.7                       | 0.13             | x,z              | 1 $^1B_1$ (x)                                  | 26.8                         | 0.03              | 88% (1,-3)                          | 1 $^1B_{3u}$ (x)                           | 27.7                         | 0.05              | 97% (1,-4)                          |
| C        | 31.3                       | 0.14             | x,z              | 2 $^1B_1$ (x)                                  | 31.4                         | 0.03              | 48% (1,-5); 39% (1,-13)             |  |                              |                   |                                     |
|          |                            |                  |                  | 3 $^1A_1$ (z)                                  | 32.2                         | 0.02              | 63% (1,-4); 15% (1,-9)              | 2 $^1B_{1u}$ (z)                           | 31.6                         | 0.02              | 64% (1,-3); 16% (1,-9)              |
|          |                            |                  |                  | 1 $^1B_2$ (y)                                  | 30.4                         | 0.09              | 30% (1,-2); 27% (1,-10)             |  |                              |                   |                                     |
| D        | 32.9                       | 1.19             | y                | 2 $^1B_2$ (y)                                  | 32.7                         | 0.29              | 58% (1,-6); 27% (1,-10)             | 1 $^1B_{2u}$ (y)                           | 32.3                         | 0.39              | 98% (1,-6)                          |
| E        | 38.8                       | 0.24             | x,z              | 4 $^1A_1$ (z)                                  | 38.2                         | 0.02              | 52% (1,-12); 25% (1,-9)             | 3 $^1B_{1u}$ (z)                           | 37.5                         | 0.02              | 53% (1,-11); 27% (1,-9)             |
|          |                            |                  |                  | 5 $^1A_1$ (z)                                  | 38.9                         | 0.02              | 53% (1,-9); 36% (1,-12)             | 4 $^1B_{1u}$ (z)                           | 38.5                         | 0.02              | 51% (1,-9); 38% (1,-11)             |
| F        | 48 <sup>h</sup>            | 0.53             | x,z              | 6 $^1B_1$ (x)                                  | 47.7                         | 0.06              | 88% (1,-17)                         | 2 $^1B_{3u}$ (x)                           | 47.1                         | 0.07              | 95% (1,-17)                         |
|          |                            |                  |                  | 7 $^1B_1$ (x)                                  | 50.0                         | 0.07              | 44% (2,-7); 23% (2,-8)              | 3 $^1B_{3u}$ (x)                           | 50.4                         | 0.09              | 78% (2,-8); 10% (3,-6)              |
| G        | 50.0                       | 0.78             | y                | 6 $^1B_2$ (y)                                  | 46.3                         | 0.02              | 36% (1,-16); 33% (1,-19)            | 2 $^1B_{2u}$ (y)                           | 46.4                         | 0.05              | 94% (1,-16)                         |
|          |                            |                  |                  | 7 $^1B_2$ (y)                                  | 47.4                         | 0.03              | 32% (1,-19); 32% (1,-16)            |  |                              |                   |                                     |
|          |                            |                  |                  | 9 $^1B_2$ (y)                                  | 50.9                         | 0.10              | 73% (3,-3); 13% (4,-7)              | 3 $^1B_{2u}$ (y)                           | 52.1                         | 0.15              | 72% (3,-4); 21% (4,-8)              |
| H        | 52.6                       | 0.91             | x,z              | 10 $^1B_1$ (x)                                 | 53.9                         | 0.10              | 51% (3,-6); 13% (2,-7)              | 4 $^1B_{3u}$ (x)                           | 54.8                         | 0.13              | 79% (3,-6)                          |

<sup>a</sup> TD-CAM-B3LYP/6-311++G(3df,3pd)// B3LYP/6-311++G(3df,3pd). Most significant transitions only; full listing is provided as supplementary data.<sup>b</sup> Peak wavenumber in 1000 cm<sup>-1</sup>.<sup>c</sup> Peak absorbance from the reduced absorbance curves  $E_{-y} = A_x - 0.3A_z$  and  $E_{-x} = A_y + 0.3A_z$  in Fig. 2.<sup>d</sup> Polarization direction, see text.<sup>e</sup> 3000 cm<sup>-1</sup> have been subtracted from the calculated wavenumbers.<sup>f</sup> Oscillator strength.<sup>g</sup> The notation (*i*,*j*) indicates a configuration generated by promotion of an electron from the *i*'th highest occupied to the *j*'th lowest unoccupied MO. Several important MOs are shown in Fig. 3.<sup>h</sup> Broad shoulder.

**Fig. 2.** Top: Reduced UV absorbance curves  $E_{-x}(\tilde{\nu}) = A_y(\tilde{\nu}) - 0.3 \cdot A_z(\tilde{\nu})$  and  $E_{-y}(\tilde{\nu}) = A_x(\tilde{\nu}) + 1.3 \cdot A_z(\tilde{\nu})$  derived from the observed LD absorbance curves  $E_U(\tilde{\nu})$  and  $E_V(\tilde{\nu})$  according to Eqns. 5. Contributions from x-polarized transitions are absent in  $E_{-x}(\tilde{\nu})$  and those from y-polarized transitions are absent in  $E_{-y}(\tilde{\nu})$ . Bottom: Graphical representation of electronic transitions predicted with TD-CAM-B3LYP for boat-shaped,  $C_{2v}$  symmetrical TTF (see Table 1). The Gaussian convolutions indicate linear combinations corresponding to the reduced absorbance curves  $E_{-x}(\tilde{\nu})$  and  $E_{-y}(\tilde{\nu})$ .

Relative to absorbance spectroscopy on isotropic samples, the additional information that can be derived from the LD curves is represented by the orientation factors  $K_i$  for the moments of the observed transitions *i* [18–23]:

$$K_i = \langle \cos^2(\vec{M}_i, U) \rangle \quad (1)$$

Here  $(\vec{M}_i, U)$  is the angle of the transition moment vector  $\vec{M}_i$  of transition *i* with the uniaxial stretching direction *U* of the polymer. The pointed brackets indicate an average over all solute molecules in the light path. A large value of the orientation factor  $K_i$  indicates efficient alignment of the transition moment  $\vec{M}_i$  with the stretching direction *U*, and vice versa. The  $K_i$  values may be determined by the graphical TEM (Trial and Error Method) procedure [18,19] which involves formation of linear combinations of  $E_U(\tilde{\nu})$  and  $E_V(\tilde{\nu})$ . Here we consider the reduced absorbance curves  $r_K(\tilde{\nu})$  [51]:

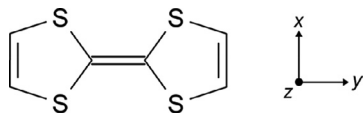
$$r_K(\tilde{\nu}) = (1 - K)E_U(\tilde{\nu}) - 2KE_V(\tilde{\nu}) \quad (2)$$

A family of curves  $r_K(\tilde{\nu})$  for TTF is shown in Fig. 1 (bottom). A spectral feature due to transition *i* vanishes from the linear combination  $r_K(\tilde{\nu})$  for  $K = K_i$  and the  $K_i$  value may thus be determined by visual inspection. In the present case of molecular  $C_{2v}$  or  $D_{2h}$  symmetry, optically allowed transitions must be polarized along the three molecular symmetry axes *x*, *y*, and *z*, corresponding to transitions to excited states of  $B_1$ ,  $B_2$ , and  $A_1$  symmetry in the case of  $C_{2v}$ , or  $B_{3u}$ ,  $B_{2u}$ , and  $B_{1u}$  symmetry in the case of  $D_{2h}$ . Hence, within experimental error, we should observe only three different  $K_i$  values equal to  $K_x$ ,  $K_y$  and  $K_z$ , the orientation factors for the three molecular axes. Moreover, the three characteristic values should add up to unity,  $K_x + K_y + K_z = 1$ .

The following orientation factors were determined in a previous IR-LD investigation of TTF aligned in stretched PE:  $(K_x, K_y, K_z) = (0.31 \pm 0.02, 0.45 \pm 0.02, 0.23 \pm 0.02)$  [52]. In that study TTF was introduced into a thick, stretched PE sample by sublimation at 60 °C for nine days. A more efficient solute alignment is achieved in the present thin sheet sample, resulting in a different distribution of the *K*-values: Inspection of the  $r_K(\tilde{\nu})$  curves in Fig. 1 (bottom) leads to  $K = 0.27$  for the feature at 26700 cm<sup>-1</sup> and  $K = 0.55$  for the one at 32900 cm<sup>-1</sup>. We assign these values to  $K_x$  and  $K_y$ , corresponding to “in-plane” short- and long axis-polarized transitions, respectively. We thus have

| MO no. | Sym. | E (eV)   |       |
|--------|------|----------|-------|
| -12    | 64   | 20 $a_1$ | 1.57  |
| -9     | 61   | 19 $a_1$ | 1.29  |
| -7     | 59   | 12 $a_2$ | 0.92  |
| -6     | 58   | 16 $b_2$ | 0.85  |
| -5     | 57   | 13 $b_1$ | 0.82  |
| -4     | 56   | 18 $a_1$ | 0.48  |
| -3     | 55   | 12 $b_1$ | 0.45  |
| -2     | 54   | 15 $b_2$ | 0.42  |
| -1     | 53   | 17 $a_1$ | 0.10  |
| 1      | 52   | 16 $a_1$ | -6.05 |
| 2      | 51   | 14 $b_2$ | -8.08 |
| 3      | 50   | 11 $a_2$ | -9.23 |

**Fig. 3.** Numbering, symmetry, and energy of molecular orbitals of boat-shape,  $C_{2v}$  symmetrical TTF predicted with CAM-B3LYP/6-311++G(3df,3pd) with indication of the orbital shape.



**Scheme 1.** Tetrathiafulvalene (TTF) and the applied coordinate system. For theoretical calculations both a planar ( $D_{2h}$ ) and boat-shape ( $C_{2v}$ ) configuration are considered.

$(K_x, K_y, K_z) = (0.27, 0.55, 0.18)$ , where  $K_z$  is obtained from the relation  $K_z = 1 - K_x - K_y$ .

While determination of the  $K$ -values may be relatively straightforward, it is far more difficult to derive the partial absorbance curves  $A_x(\tilde{\nu})$ ,  $A_y(\tilde{\nu})$ , and  $A_z(\tilde{\nu})$  corresponding to absorbance polarized along the three symmetry axes of the molecule. In general, the three partial absorbance curves cannot be determined from only two linearly independent spectra  $E_U(\tilde{\nu})$  and  $E_V(\tilde{\nu})$ . We shall adopt the formalism outlined by Madsen et al. [51] and construct the pair of reduced absorbance curves

$E_{-x}(\tilde{\nu})$  and  $E_{-y}(\tilde{\nu})$ :

$$\begin{aligned} E_{-x}(\tilde{\nu}) &= (K_y - K_x)^{-1} r_{K_x}(\tilde{\nu}) \\ E_{-y}(\tilde{\nu}) &= (K_x - K_y)^{-1} r_{K_y}(\tilde{\nu}) \end{aligned} \quad (3)$$

Contributions from  $x$ -polarized transitions are absent in  $E_{-x}(\tilde{\nu})$  and those of  $y$ -polarized transitions are absent in  $E_{-y}(\tilde{\nu})$ . The resulting curves produced with  $(K_x, K_y) = (0.27, 0.55)$  are shown in Fig. 2 (top). They are related to the partial absorbance curves  $A_x(\tilde{\nu})$ ,  $A_y(\tilde{\nu})$ , and  $A_z(\tilde{\nu})$  through the relations [51]:

$$\begin{aligned} E_{-x}(\tilde{\nu}) &= A_y(\tilde{\nu}) + \frac{K_z - K_x}{K_y - K_x} A_z(\tilde{\nu}) \\ E_{-y}(\tilde{\nu}) &= A_x(\tilde{\nu}) + \frac{K_z - K_y}{K_x - K_y} A_z(\tilde{\nu}) \end{aligned} \quad (4)$$

For many planar or nearly planar chromophores, “out-of-plane” polarized absorbance such as  $A_z(\tilde{\nu})$  can to a good approximation be set equal to zero in the near UV region, yielding directly  $E_{-x}(\tilde{\nu}) = A_y(\tilde{\nu})$  and  $E_{-y}(\tilde{\nu}) = A_x(\tilde{\nu})$ . However, this is not possible with TTF where the three partial absorbance curves all contribute significantly to the observed spectrum (see below). TTF can thus be characterized as a “three-dimensional” chromophore. With  $(K_x, K_y, K_z) = (0.27, 0.55, 0.18)$  we obtain:

$$\begin{aligned} E_{-x}(\tilde{\nu}) &= A_y(\tilde{\nu}) - 0.3 \cdot A_z(\tilde{\nu}) \\ E_{-y}(\tilde{\nu}) &= A_x(\tilde{\nu}) + 1.3 \cdot A_z(\tilde{\nu}) \end{aligned} \quad (5)$$

As discussed in the following,  $E_{-x}(\tilde{\nu})$  and  $E_{-y}(\tilde{\nu})$  provide a useful representation of the observed polarization data for TTF.

#### 4.2. Electronic transitions

The reduced absorbance curves  $E_{-x}(\tilde{\nu})$  and  $E_{-y}(\tilde{\nu})$  are shown in Fig. 2 (top) with indication of prominent features A to H. As explained above and indicated in Eqns. 5, the curves  $E_{-x}(\tilde{\nu})$  and  $E_{-y}(\tilde{\nu})$  contain linear combinations of the partial absorbance curves  $A_x(\tilde{\nu})$ ,  $A_y(\tilde{\nu})$ , and  $A_z(\tilde{\nu})$ . But for simplicity, features in  $E_{-x}(\tilde{\nu})$  are in the following described as “long axis-polarized” and those in  $E_{-y}(\tilde{\nu})$  as “short axis-polarized”. The bottom panel of Fig. 2 shows transitions predicted for the boat-shape  $C_{2v}$  symmetrical equilibrium geometry, as well as corresponding convoluted curves constructed to correspond to the reduced absorbance curves  $E_{-x}(\tilde{\nu})$  and  $E_{-y}(\tilde{\nu})$  according to Eqns. 5. The observed features and the suggested assignments to predicted electronic transitions are listed in Table 1.

The absorption spectrum of TTF starts with a weak transition A with a maximum at 22,000  $\text{cm}^{-1}$  (455 nm), responsible for the red color of the substance. The band is primarily long axis-polarized, but the observed polarization of this very weak absorbance is probably determined by intensity borrowed from stronger transitions at higher energy, such as those giving rise to the intense, long axis-polarized band D (see below). Band A must be assigned to the optically very weak  $2^1A_1$  state predicted at 21,000  $\text{cm}^{-1}$ . This state is dominated by the HOMO-LUMO excitation involving promotion of an electron from 16 $a_1$  to 17 $a_1$  (Fig. 3). This is essentially a  $\pi$ - $\sigma^*$  transition, although  $\pi$  and  $\sigma$  type contributions are more or less mixed in the boat-shape  $C_{2v}$  symmetrical equilibrium conformation. The present assignment of band A is consistent with previous assignments, such as those by Andreu et al. [15] and Pou-Amérgo et al. [16,17].

The relatively intense feature B observed at 26,700  $\text{cm}^{-1}$  (375 nm) is short axis-polarized. The feature overlaps the onset of the long axis-polarized band D and probably contains long axis-polarized contributions due to vibronic interaction with this strong band. Band B is easily assigned to the  $x$ -polarized electronic transition to the  $1^1B_1$  state predicted at 26,800  $\text{cm}^{-1}$ . This is essentially a  $\pi$ - $\pi^*$  transition involving promotion from 16 $a_1$  to 12 $b_1$  (Fig. 3). Again, this assignment is consistent with previous assignments [15–17].

The following feature C at 31,300  $\text{cm}^{-1}$  (320 nm) was not clearly observed in previous experimental studies, largely due to overlap with the strong absorbance D; it does not seem to have been discussed in detail



in previous literature. It is short axis-polarized and can be assigned to overlapping contributions from the states  $2^1B_1$  and  $3^1A_1$  predicted at 31,400 and 32,200  $\text{cm}^{-1}$ , giving rise to *x*- and *z*-polarized intensity, respectively. The orbital origins of the computed transitions are complex, as indicated in Table 1. Wavenumber and intensity of the predicted  $3^1A_1$  state depend significantly on the inclusion of diffuse functions in the basis set (S6), indicating a substantial component of non-valence character. Pou-Amérigo and co-workers predicted Rydberg states from about 30,000  $\text{cm}^{-1}$  and above, but with low oscillator strengths [16,17].

The strong, long axis-polarized feature *D* peaking at 32,900  $\text{cm}^{-1}$  (304 nm) is the most intense absorption band in the investigated spectral region. It displays a prominent shoulder close to 31,500  $\text{cm}^{-1}$  (317 nm). This composite band can be assigned to overlapping contributions from transitions to the  $1^1B_2$  and  $2^1B_2$  states computed at 30,400 and 32,700  $\text{cm}^{-1}$  with oscillator strengths 0.09 and 0.29, respectively (Table 1). Pou-Amérigo et al. [17] calculated corresponding  $1^1B_2$  and  $2^1B_2$  states at 32,300 and 34,400  $\text{cm}^{-1}$  with TD-B3P86/aug-cc-pVDZ.

The tail of band *D* overlaps the short axis-polarized feature *E* with a maximum at 38,800  $\text{cm}^{-1}$  (258 nm). This absorbance has apparently not previously been discussed in any detail. According to the present theoretical results, the feature *E* can be assigned to the states  $4^1A_1$  and  $5^1A_1$  predicted at 38,200 and 38,900  $\text{cm}^{-1}$ , giving rise to transitions polarized along the “out-of-plane” *z* axis. Prediction of the  $4^1A_1$  and  $5^1A_1$  states depend strongly on inclusion of diffuse functions in the basis set (S6), indicating that the states have significant non-valence character. The transitions are primarily due to promotions to the virtual orbitals  $19a_1$  and  $20a_1$  (−9 and −12 in Table 1) which have large *d* and *s* type Rydberg character, respectively, see Fig. 3. The predictions are supported by the results of calculations with larger basis sets and with other functionals (S7 – S11), although the computed relative optical intensities of the  $4^1A_1$  and  $5^1A_1$  states depend on the model.

The vacuum UV region exhibits overlapping long and short axis-polarized intense absorbance. Assignment of the observed features to the numerous transitions calculated in this region is necessarily tentative. The short axis-polarized absorbance is characterized by a very broad band with maximum *H* close to 53,900  $\text{cm}^{-1}$  (186 nm) and a prominent shoulder *F* at 48,000  $\text{cm}^{-1}$  (210 nm). This absorbance can be assigned to several states, such as the  $6^1B_1$ ,  $7^1B_1$ , and  $10^1B_1$  states predicted at 47,700, 50,000, and 53,900  $\text{cm}^{-1}$  (Table 1). The long axis-polarized absorbance *G* peaking at 50,000  $\text{cm}^{-1}$  (200 nm) can be assigned to the  $9^1B_1$  state predicted at 50,900  $\text{cm}^{-1}$ , with contributions also from the  $6^1B_2$  and  $7^1B_2$  states calculated at 46,300 and 47,400  $\text{cm}^{-1}$  (Table 1). But it must be emphasized that diffuse functions in the basis set have a profound impact on the absorption profiles predicted in the vacuum UV region (S6), suggesting significant non-valence character of several transitions. The applied theoretical model is likely to be less accurate in this region.

In the preceding paragraphs, the observed absorption bands of TTF are discussed with reference to theoretical transitions calculated for the boat-shape  $C_{2v}$  symmetrical equilibrium nuclear configuration. Table 1 also lists the transitions calculated for the planar  $D_{2h}$  symmetrical molecular geometry, and a comparison of the computed spectra is provided in S5. It is apparent that the predicted spectra show obvious similarities, but also significant differences. In particular, the  $1^1B_2$  and  $2^1B_1$  states of boat-shape TTF predicted at 30,400 and 31,400  $\text{cm}^{-1}$  correspond to optically forbidden states in the planar  $D_{2h}$  geometry.

## 5. Conclusions

Tetrathiafulvalene (TTF), a compound with a diverse field of applications in both molecular electronics and supramolecular chemistry, has been characterized in detail with respect to electronic states in the near- and vacuum-UV region using synchrotron radiation polarization spectroscopy. Interpretation of the experimental linear dichroic absorbance data show that TTF is a truly 3-dimensional chromophore with UV spectral contributions from electronic transitions polarized along all three

molecular axes. These findings may be of importance in functional applications relying on TTF-derived compounds e.g. in photoresponsive conducting materials [53]. The LD analysis allowed for resolution of eight distinct spectral features, several of which were overlapping and previously unrecognized. Theoretical calculations of electronic transitions for both the non-planar  $C_{2v}$  symmetrical equilibrium geometry and the planar  $D_{2h}$  geometry were performed using TD-DFT models. Considering the low barrier of the  $D_{2h}$  transition state, TTF must be considered a dynamic chromophore that likely undergoes rapid fluctuation, flipping between two  $C_{2v}$  conformations. Such behavior can most likely contribute to the diffuseness of the bands observed in the UV spectrum, and may also via consideration of vibronic coupling have implications for the molecular electronic properties of TTF-derived compounds, as discussed for certain salts [54]. We find in general that there is a good agreement between experimental transitions in the low-energy region <40,000  $\text{cm}^{-1}$  (>250 nm) to the results consistently obtained with a selection of different TD-DFT models and basis sets and a reasonable agreement in the high-energy region. However, the DFT calculations did show that diffuse basis set functions were essential for a reliable prediction of several transitions, perhaps due to their Rydberg-like characteristics. More advanced theoretical approaches are required for a more complete understanding of the electronic transitions, particularly concerning the high-energy region (>40,000  $\text{cm}^{-1}$ ) with a proper treatment of Rydberg states in an approach that can also accommodate the dynamic nature of the chromophore.

## Declaration of Competing Interest

The authors declare that they have no known competing financial interests or personal relationships that could have appeared to influence the work reported in this paper.

## Acknowledgments

The authors acknowledge a beamtime grant for synchrotron radiation linear dichroism spectroscopy at ISA, the Centre for Storage Rings Facilities at Aarhus University. We are grateful for technical assistance from Eva M. Karlsen, Roskilde University, and we thank Prof. Mogens Brøndsted Nielsen from the University of Copenhagen for advice and input during the preparation of the manuscript.

## Supplementary materials

Supplementary material associated with this article can be found, in the online version, at doi:10.1016/j.chphi.2020.100009.

## References

- [1] K. Bechgaard, C.S. Jacobsen, K. Mortensen, H.J. Pedersen, N. Thorup, The properties of five highly conductive salts: (TMTSF) $2X$ ,  $X = PF_6^-$ ,  $AsF_6^-$ ,  $SbF_6^-$ ,  $BF_4^-$  and  $NO_3^-$ , derived from Tetrathiafulvalene (TMTSF), Solid State Commun. 33 (1980) 1119–1125.
- [2] D. Jérôme, A. Mazaud, M. Ribault, K. Bechgaard, Superconductivity in a synthetic organic conductor (TMTSF) $2PF_6$ , J. Phys. Lett. 41 (1980) 95–98.
- [3] N. Martín, Tetrathiafulvalene: the advent of organic metals, Chem. Commun. 49 (2013) 7025–7027.
- [4] A. Aviram, M.A. Ratner, Molecular rectifiers, Chem. Phys. Lett. 29 (1974) 277–283.
- [5] G. Ho, J.R. Heath, M. Kondratenko, D.F. Perepichka, K. Arseneault, M. Pérolet, M.R. Bryce, The first studies of a Tetrathiafulvalene- $\sigma$ -acceptor molecular rectifier, Chem. - A Eur. J. 11 (2005) 2914–2922.
- [6] T. Ikeda, J.F. Stoddart, Electrochromic materials using mechanically interlocked molecules, Sci. Technol. Adv. Mater. 9 (2008) 014104.
- [7] D. Canavet, M. Sallé, G. Zhang, D. Zhang, D. Zhu, Tetrathiafulvalene (TTF) derivatives: key building-blocks for switchable processes, Chem. Commun. (2009) 2245–2269.
- [8] A. Jana, S. Bähring, M. Ishida, S. Goeb, D. Canavet, M. Sallé, J.O. Jeppesen, J.L. Sessler, Functionalised tetrathiafulvalene- (TTF-) macrocycles: recent trends in applied supramolecular chemistry, Chem. Soc. Rev. 47 (2018) 5614–5645.
- [9] H.V. Schröder, C.A. Schalley, Tetrathiafulvalene – a redox-switchable building block to control motion in mechanically interlocked molecules, Beilstein J. Org. Chem. 14 (2018) 2163–2185 and references cited therein.

- [10] D.L. Coffen, J.Q. Chambers, D.R. Williams, P.E. Garrett, N.D. Canfield, Tetrathioethylenes, *J. Amer. Chem. Soc.* 93 (1971) 2258–2268.
- [11] R. Zahradník, P. Čárský, S. Hünig, G. Kiesslich, D. Scheutzw, Conjugated radicals. VII. Tetrathiofulvalene and a note on sulfur-containing conjugated radicals, *Int. J. Sulfur Chem. C6* (1971) 109–122.
- [12] R. Gleiter, E. Schmidt, D.O. Cowan, J.P. Ferraris, The electronic structure of tetrathiofulvalene, *J. Electron Spectrosc. Relat. Phenomena* 2 (1973) 207–210.
- [13] R. Gleiter, M. Kobayashi, J. Spanget-Larsen, J.P. Ferraris, A.N. Bloch, K. Bechgaard, D.O. Cowan, Photoelectron and electronic absorption spectra of tetrathiofulvalene and related compounds, *Ber. Bunsenges. physik. Chem.* 79 (1975) 1218–1226.
- [14] J. Spanget-Larsen, R. Gleiter, S. Hünig, The electronic structure of dibenzotetrathiofulvalene, *Chem. Phys. Lett.* 37 (1976) 29–32.
- [15] R. Andreu, J. Garín, J. Orduna, Electronic absorption spectra of closed and open-shell tetrathiofulvalenes: the first time-dependent density-functional study, *Tetrahedron* 57 (2001) 7883–7892.
- [16] R. Pou-Américo, E. Ortí, M. Merchán, M. Rubio, P.M. Viruela, Electronic Transitions in Tetrathiofulvalene and Its Radical Cation: a Theoretical Contribution, *J. Phys. Chem. A* 106 (2002) 631–640.
- [17] R. Pou-Américo, P.M. Viruela, R. Viruela, M. Rubio, E. Ortí, Electronic spectra of tetrathiofulvalene and its radical cation: analysis of the performance of the time-dependent DFT approach, *Chem. Phys. Lett.* 352 (2002) 491–498.
- [18] J. Michl, E.W. Thulstrup, in: *Spectroscopy With Polarized light: Solute Alignment By photoselection, in Liquid crystals, polymers, and Membranes*, VCH-Wiley, Deerfield Beach, FL, 1986, p. 1995.
- [19] E.W. Thulstrup, J. Michl, *Elementary Polarization Spectroscopy*, Wiley-VCH, New York, Weinheim, 1989.
- [20] A. Rodger, B. Nordén, *Circular Dichroism and Linear Dichroism*, Oxford University Press, UK, 1997.
- [21] E.W. Thulstrup, P.W. Thulstrup, Polarization spectroscopic studies of ordered samples, *Acta Chim. Slov.* 52 (2005) 371–383.
- [22] P.W. Thulstrup, E.W. Thulstrup, Information content in linear dichroism spectra, *Polish J. Chem.* 82 (2008) 901–920.
- [23] B. Nordén, A. Rodger, T. Dafforn, *Linear Dichroism and Circular Dichroism*, RSC Publishing, Cambridge, UK, 2010.
- [24] M.E. Casida, Review: time-dependent density-functional theory for molecules and molecular solids, *J. Mol. Struct. Theochem* 914 (2009) 3–18.
- [25] C. Adamo, D. Jacquemin, The calculations of excited-state properties with time-dependent density functional theory, *Chem. Soc. Rev.* 42 (2013) 845–856.
- [26] J.B. Foresman, Æ. Frisch, *Exploring Chemistry With Electronic Structure Methods*, Gaussian, Inc., Wallingford CT, 2015 Third Edition.
- [27] S.C. Nguyen, B.K.V. Hansen, S.V. Hoffmann, J. Spanget-Larsen, Electronic states of emodin and its conjugate base. Synchrotron linear dichroism spectroscopy and quantum chemical calculations, *Chem. Phys.* 352 (2008) 167–174.
- [28] D.D. Nguyen, N.C. Jones, S.V. Hoffmann, J. Spanget-Larsen, Synchrotron radiation linear dichroism (SRLD) investigation of the electronic transitions of quinzarin, chrysazin, and anthrarufin, *Spectrochim. Acta Part A* 77 (2010) 279–286.
- [29] P.W. Thulstrup, S.V. Hoffmann, B.K.V. Hansen, J. Spanget-Larsen, Unique interplay between electronic states and dihedral angle for the molecular rotor diphenyl-diacyetylene, *Phys. Chem. Chem. Phys.* 13 (2011) 16168–16174.
- [30] D.D. Nguyen, N.C. Jones, S.V. Hoffmann, S.H. Andersen, P.W. Thulstrup, J. Spanget-Larsen, Electronic states of 1,4-bis(phenylethynyl)benzene: a synchrotron radiation linear dichroism investigation, *Chem. Phys.* 392 (2012) 130–135.
- [31] P.W. Thulstrup, N.C. Jones, S.V. Hoffmann, J. Spanget-Larsen, Electronic states of the fluorophore 9,10-bis(phenylethynyl)anthracene (BPEA). A synchrotron radiation linear dichroism investigation, *Chem. Phys. Lett.* 559 (2013) 35–40.
- [32] D.D. Nguyen, N.C. Jones, S.V. Hoffmann, J. Spanget-Larsen, Vacuum UV polarization spectroscopy of *p*-Terphenyl, *J. Phys. Chem. A* 122 (2018) 184–191.
- [33] D.D. Nguyen, N.C. Jones, S.V. Hoffmann, J. Spanget-Larsen, Electronic states of dibenzo-*p*-dioxin. A synchrotron radiation linear dichroism investigation, *Chem. Phys.* 519 (2019) 64–68.
- [34] D.D. Nguyen, N.C. Jones, S.V. Hoffmann, J. Spanget-Larsen, UV synchrotron radiation linear dichroism spectroscopy of the antipsoriatic drug anthralin, *PeerJ. Phys. Chem.* 1 (2019) e5, doi:10.7717/peerj-pchem.5.
- [35] A.J. Miles, S.V. Hoffmann, Y. Tao, R.W. Janes, B.A. Wallace, Synchrotron radiation circular dichroism (SRCD) spectroscopy: new beamlines and new applications in biology, *Spectroscopy* 21 (2007) 245–255.
- [36] A.J. Miles, R.W. Janes, A. Brown, D.T. Clarke, J.C. Sutherland, Y. Tao, B.A. Wallace, S.V. Hoffmann, Light flux density threshold at which protein denaturation is induced by synchrotron radiation circular dichroism beamlines, *J. Synchrotron Radiat.* 15 (2008) 420–422.
- [37] M.H. Palmer, T. Ridley, S.V. Hoffmann, N.C. Jones, M. Coreno, M. De Simone, C. Grazioli, M. Biczysko, A. Baiardi, P. Limao-Vieira, Interpretation of the vacuum ultraviolet photoabsorption spectrum of iodobenzene by ab initio computations, *J. Chem. Phys.* 142 (2015) 132302.
- [38] M.J. Frisch, G.W. Trucks, H.B. Schlegel, G.E. Scuseria, M.A. Robb, J.R. Cheeseman, G. Scalmani, V. Barone, B. Mennucci, G.A. Petersson, H. Nakatsuji, M. Caricato, X. Li, H.P. Hratchian, A.F. Izmaylov, J. Bloino, G. Zheng, J.L. Sonnenberg, M. Hada, M. Ehara, K. Toyota, R. Fukuda, J. Hasegawa, M. Ishida, T. Nakajima, Y. Honda, O. Kitao, H. Nakai, T. Vreven, J.A. Montgomery Jr., J.E. Peralta, F. Ogliaro, M. Bearpark, J.J. Heyd, E. Brothers, K.N. Kudin, V.N. Staroverov, T. Keith, R. Kobayashi, J. Normand, K. Raghavachari, A. Rendell, J.C. Burant, S.S. Iyengar, J. Tomasi, M. Cossi, N. Rega, J.M. Millam, M. Klene, J.E. Knox, J.B. Cross, V. Bakken, C. Adamo, J. Jaramillo, R. Gomperts, R.E. Stratmann, O. Yazyev, A.J. Austin, R. Cammi, C. Pomelli, J.W. Ochterski, R.L. Martin, K. Morokuma, V.G. Zakrzewski, G.A. Voth, P. Salvador, J.J. Dannenberg, S. Dapprich, A.D. Daniels, O. Farkas, J.B. Foresman, J.V. Ortiz, J. Cioslowski, D.J. Fox, *Gaussian 09, Revision D.01* (2013).
- [39] M.J. Frisch, G.W. Trucks, H.B. Schlegel, G.E. Scuseria, M.A. Robb, J.R. Cheeseman, G. Scalmani, V. Barone, G.A. Petersson, H. Nakatsuji, X. Li, M. Caricato, A.V. Marenich, J. Bloino, B.G. Janesko, R. Gomperts, B. Mennucci, H.P. Hratchian, J.V. Ortiz, A.F. Izmaylov, J.L. Sonnenberg, D. Williams-Young, F. Ding, F. Lipparini, F. Egidi, J. Goings, B. Peng, A. Petrone, T. Henderson, D. Ranasinghe, V.G. Zakrzewski, J. Gao, N. Rega, G. Zheng, W. Liang, M. Hada, M. Ehara, K. Toyota, R. Fukuda, J. Hasegawa, M. Ishida, T. Nakajima, Y. Honda, O. Kitao, H. Nakai, T. Vreven, K. Throssell, J.A. Montgomery, Jr., J.E. Peralta, F. Ogliaro, M.J. Bearpark, J.J. Heyd, E.N. Brothers, K.N. Kudin, V.N. Staroverov, T.A. Keith, R. Kobayashi, J. Normand, K. Raghavachari, A.P. Rendell, J.C. Burant, S.S. Iyengar, J. Tomasi, M. Cossi, J.M. Millam, M. Klene, C. Adamo, R. Cammi, J.W. Ochterski, R.L. Martin, K. Morokuma, O. Farkas, J.B. Foresman, D.J. Fox, *Gaussian16, Revision A.03*, Gaussian, Inc., Wallingford CT, 2016.
- [40] A.D. Becke, Density-functional thermochemistry. III. The role of exact exchange, *J. Chem. Phys.* 98 (1993) 5648–5652.
- [41] C. Lee, W. Yang, R.G. Parr, Development of the Colle-Salvetti correlation-energy formula into a functional of the electron density, *Phys. Rev. B* 37 (1988) 785–789.
- [42] I. Hargittai, J. Brunvoll, M. Kolonits, V. Khodorkovsky, Tetrathiofulvalene: gas-phase molecular structure from electron diffraction, *J. Mol. Struct.* 317 (1994) 273–277.
- [43] R. Viruela, P.M. Viruela, R. Pou-Américo, E. Ortí, Flexibility of TTF. A theoretical study, *Synth. Met.* 103 (1999) 1991–1992.
- [44] V. Mukherjee, N.P. Singh, Theoretical vibrational spectra and thermodynamics of organic semiconductive tetrathiofulvalene and its cation radical, *Spectrochim. Acta A* 117 (2014) 315–322.
- [45] T. Yanai, D. Tew, N.A. Handy, New hybrid exchange-correlation functional using the Coulomb-attenuating method (CAM-B3LYP), *Chem. Phys. Lett.* 393 (2004) 51–57.
- [46] T.H. Dunning Jr., Gaussian basis sets for use in correlated molecular calculations. I. The atoms boron through neon and hydrogen, *J. Chem. Phys.* 90 (1989) 1007–1023.
- [47] D.E. Woon, T.H. Dunning Jr., Gaussian-basis sets for use in correlated molecular calculations. 3. The atoms aluminum through argon, *J. Chem. Phys.* 98 (1993) 1358–1371.
- [48] Y. Tawada, T. Tsuneda, S. Yanagisawa, T. Yanai, K. Hirao, A long-range-corrected time-dependent density functional theory, *J. Chem. Phys.* 120 (2004) 8425.
- [49] O.A. Vydrov, J. Heyd, A. Kruckau, G.E. Scuseria, Importance of short-range versus long-range Hartree-Fock exchange for the performance of hybrid density functionals, *J. Chem. Phys.* 125 (2006) 074106.
- [50] J.-D. Chai, M. Head-Gordon, Long-range corrected hybrid density functionals with damped atom-atom dispersion corrections, *Phys. Chem. Chem. Phys.* 10 (2008) 6615–6620.
- [51] F. Madsen, I. Terpager, K. Olskaer, J. Spanget-Larsen, Ultraviolet-visible and infrared linear dichroism spectroscopy of 1,8-dihydroxy-9,10-anthraquinone aligned in stretched polyethylene, *Chem. Phys.* 165 (1992) 351–360.
- [52] K. Troels-Smith, Master Thesis (in Danish), Roskilde University, 1995.
- [53] K. Tsujimoto, R. Ogasawara, Y. Kishi, H. Fujiwara, TTF-fluorene dyads and their M(CN)<sub>2</sub>– (M = Ag, Au) salts designed for photoresponsive conducting materials, *New J. Chem.* 38 (2014) 406–418.
- [54] K. Tokunaga, Forces in EDO-TTF: theoretical study of isotope and charge effects on vibronic coupling, *Phys. Procedia* 14 (2011) 152–163.